# Reactions of Hydrazoic Acid and Trimethylindium on $TiO_2$ Rutile (110) Surface: A Computational Study on the Formation of the First Monolayer InN

**Jeng-Han Wang and M. C. Lin***

*Department of Chemistry, Emory University, Atlanta, Georgia 30322*

*Received: October 4, 2005; In Final Form: December 5, 2005*

This Article reports the result of a computational study on the reaction of hydrazoic acid and trimethylindium (TMIn), coadsorbed on $TiO_2$ rutile (110) surface. The adsorption geometries and energies of possible adsorbates including $HN_3-In(CH_3)_3(a)$ and its derivatives, $HN_3-In(CH_3)_2(a)$, $N_3-In(CH_3)_2(a)$, $N_3-In(CH_3)(a)$, and N−In(a), have been predicted by first-principles calculations based on the density functional theory (DFT) and the pseudopotential method. The mechanisms of these surface reactions have also been explicitly elucidated with the computed potential energy surfaces. Starting from the interaction of three stable $HN_3$ adsorbates, $HN_3-O_b(a)$, $H(N_2)N-O_b(a)$, and $Ti-NN(H)N-O_b(a)$, where $O_b$ is the bridged O site on the surface, with two stable intermediates from the adsorption and dissociative adsorption of TMIn, $(H_3C)_3In-O_b(a)$ and $(H_3C)_2In-O_b(a) + H_3C-O_b(a)$, InN products can be formed exothermically via four reaction paths following the initial barrierless In-atom association with the N atom directly bonded to H, by $CH_4$ elimination (with ~40 kcal/mol barriers), the InN−N bond breaking and the final $CH_3$ elimination or migration (with <20 kcal/mol barriers). These Langmuir−Hinshelwood processes producing the two most stable InN(a) side-on adsorptions confirm that $HN_3$ and TMIn are indeed very efficient precursors for the deposition of InN films on $TiO_2$ nanoparticles. The result of similar calculations for the reactions occurring by the Rideal−Eley mechanism involving $HN_3(a)$ + TMIn(g) and $HN_3(g)$ + TMIn(a) indicates that they are energetically less favored and produce the less stable InN(a) with end-on configurations.

## 1. Introduction

$TiO_2$ has been widely studied because of its unique photochemical characteristics for potential applications spanning from photocatalysis to wet solar cells and photoelectrochemical water splitting.[1−5] Recently, deposition of InN films of varying thickness on $TiO_2$ nanoparticle films has been demonstrated by low-pressure organometallic chemical vapor deposition (OMCVD)[6] near 700 K with continuous UV irradiation using hydrazoic acid ($HN_3$) and trimethylindium (TMIn), which are perhaps the most efficient precursors.[7−9] The resulting InN film on $TiO_2$ exhibits a broad UV/visible absorption between 390 and 800 nm quite similar to that of Graetzel's "black" dye,[10] indicating a promising possibility for photovoltaic applications.

To understand the mechanism of the OMCVD process producing the InN film, the reactions of the individual precursors on the $TiO_2$ surface have been experimentally studied by FTIR spectroscopy, monitoring the effects of dosage, UV irradiation and heating, and have also been computationally modeled with first-principles calculations for adsorption energies, vibrational frequencies of adspecies and potential energy surfaces of the adsorption and decomposition processes.[11,12]

In the $HN_3/TiO_2$ system,[12] both the molecular ($HN_3(a)$) and dissociated adspecies, $N_3(a)$ and H(a), with different adsorption structures, such as end-on and side-on configurations, were observed by FTIR spectroscopy under the conditions of high $HN_3$ dosage at room temperature and have been confirmed by the optimized structures computationally. Similar results have been reported in some other systems involving $HN_3(a)$ on polycrystalline gold,[13] amorphous ice[13] and C(100)[14] surfaces with similar experimental conditions. Upon UV irradiation or at higher surface temperatures, only the atomic N-adsorbates can ultimately survive on the $TiO_2$ surface; this is also similar to the behavior of $HN_3$ on GaAs,[15] Si(100)-2 × 1,[16,17] Si(111)-7 × 7[18] and Al(111)[19] surfaces.

In the TMIn/$TiO_2$ system,[11] the dosage and UV irradiation dependent experiments in the absence of oxygen showed that the methyl groups of the adsorbed TMIn(a), solely on the bridged O-atom sites, can migrate on the surface at room temperature or by UV photons because of the weak $In-CH_3$ and the strong $O-CH_3$ bonds with the bridged O atom. The decomposition of the first $In-CH_3$ bond producing $(CH_3)_2In(a) + CH_3O(a)$ was found to have a low barrier and be highly exothermic. Further decomposition of the TMIn(a) fragments, $(CH_3)_2In(a)$, $(CH_3)In(a)$, $H_3C(a)$ can produce $CH_x$-(a), C(a), H(a) and In(a) adspecies, at higher surface temperatures. Similar results were also observed in TMIn reactions on other surfaces of Si(111),[20,21] quartz,[22,23] and GaAs(100).[24−27] In the experiments with UV irradiation in the presence of oxygen, the methyl groups of $(CH_3)_xIn(a)$ can be readily oxidized to methoxy and carboxyl groups. This result is attributable to the photocatalytic effects of $TiO_2$ nanoparticles and is consistent with similar photooxidation results of dimethyl methylphosphonate,[28] methanol,[29] ethanol,[30] and methylamine[31] on $TiO_2$ nanoparticle films.

In this paper, we have investigated reactions of $HN_3$ and TMIn coadsorbed on the $TiO_2$ rutile (110) surface forming InN(a) computationally. The objective of the present study lies in elucidating the mechanism of the InN formation on the surface under similar conditions employed in the low-pressure

* To whom correspondence should be addressed. E-mail: chemmcl@emory.edu.

10.1021/jp055659b CCC: $33.50 
Published on Web 01/19/2006

OMCVD experiment.[6] Section 2 describes the computational method employed in current study. The computational results, which include the optimized adsorbate structures, adsorption energies and potential energy surfaces, are reported in section 3. This paper is concluded in section 4 with a brief summary.

## 2. Computational Method

The Vienna ab initio Simulation Package (VASP),[32−35] implementing the density functional theory (DFT), has been employed for the geometrical structure optimization and total energy computation. The exchange-correlation function is treated with the local-density approximation (LDA)[36] and the Perdew−Wang 1991 (PW91) formulation,[37] which works well for surfaces,[38] is employed with the generalized gradient approximation (GGA)[37,39] for total energy calculations. The core electron calculations are applied with pseudopotentials implemented in VASP. The valance electrons for the $TiO_2$ model, the ten 3p, 3d and 4s electrons of each Ti atom and the six 2s and 2p electrons of each O atom are expanded with a plane-wave basis set. The plane-wave expansion includes all plane waves with their kinetic energies smaller than the chosen cutoff energy, $\hbar K^2/2m < E_{cut}$, which ensures the convergence with respect to the basis set. For the adsorbates, the five 2s and 2p electrons of each N atom, the one 1s electron for the H atom, the four 2s and 2p electrons of each C atom and the three 5s and 5p electrons of each In atom are also explicitly considered in the same way.

The $TiO_2$ nanoparticle film is a polycrystalline material with different $TiO_2$ surface structures. The (101) and (110) surfaces of anatase and rutile, respectively, have the lowest surface energies with similar characteristics;[40] they may coexist in the nanoparticle film. The annealing treatment to clean the film before each experiment as aforementioned may transform more anatase to rutile because of the small particle size.[41,42] Besides, the reactions of $HN_3$ and TMIn on $TiO_2$ rutile (110) surface have recently been calculated individually.[11,12] The $TiO_2$ rutile (110) surface model, therefore, is employed in the present simulation with $HN_3$ and TMIn coadsorbed on the surface for the formation of InN.

The periodic surface is simulated by the repeated supercells in three directions. Repetition of the in-plane supercells creates an infinite slab, whereas periodicity in the direction perpendicular to the slab creates an infinite stack of slabs. The supercell geometry used in this study consists of 16 [$TiO_2$] units with the bond lengths and angles, initially defined according to the experimental result,[43] as shown in Figure 1. The lower part of the supercells is fixed at the optimized lattice constants, and a certain vacuum region is used to separate the top and bottom surfaces of the slabs to minimize the interaction between distinct slab surfaces in this infinitely periodic model system. The Brillouin zone is sampled with the chosen Monkhorst−Pack[44] *k*-point, which also ensures the convergence of the whole system. The transition states for dissociative adsorptions are located by a series of elastic bands using the NEB method.[45]

## 3. Results and Discussion

**3.1. Computational Condition Tests.** To ensure the reliability of the computational results, the method and parameters employed in the current study have first been examined by optimizing the bulk $TiO_2$ in the rutile phase, which is tetragonal, and by characterizing its lattice constants, *a* and *c*. At the 600 eV cutoff energy and 4 × 5 × 4 Monkhorst−Pack[44] *k*-point settings, the calculated lattice parameters, $a = 4.593$ Å and $c = 2.933$ Å, and internal coordinate, 0.296, have about 1% deviation from the experimental data.[43] With the acceptable accuracy, the conditions are then applied for the $TiO_2$ rutile (110) surface model and employed in the simulation of surface reactions.

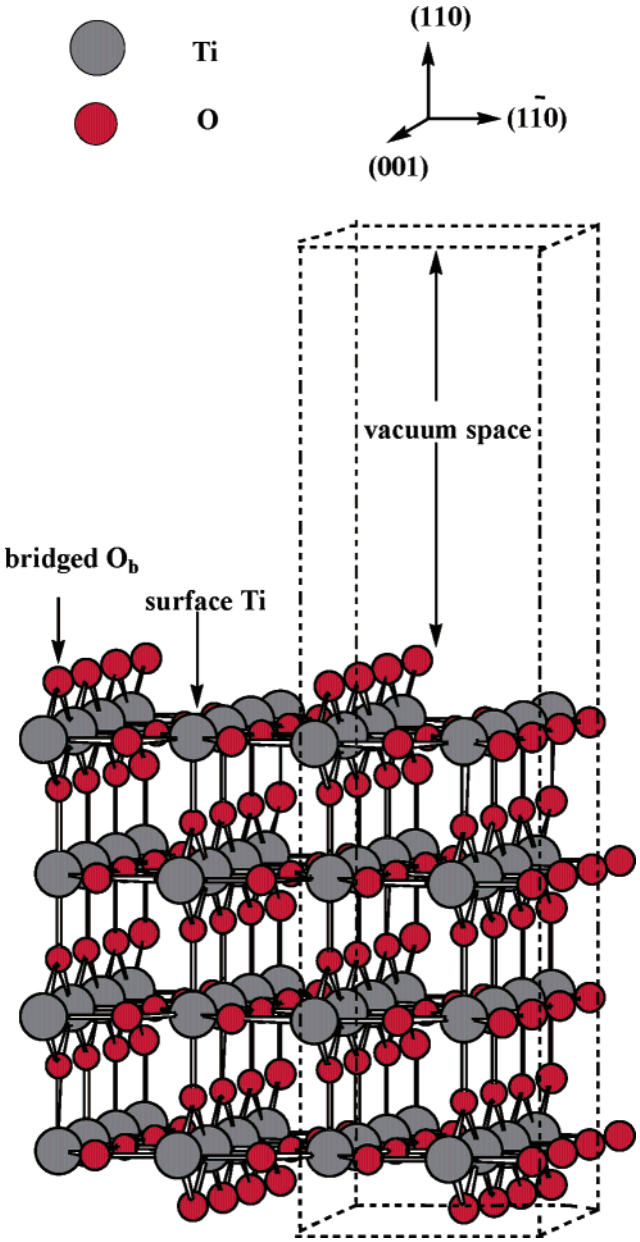


**Figure 1.** Perspective view of the $TiO_2$(110) surface. The dashed lines indicate the supercell used in the slab calculations.

As shown in Figure 1, the $TiO_2$(110) surface is modeled as an infinite slab and the periodic boundary conditions are applied. The surface supercell has dimensions of $\sqrt{2}a$ x *c* along the (1$\bar{1}$0) and (001) directions, where *a* and *c* are the lattice constants of the bulk $TiO_2$ unit cell. The slab thickness is related to the number of layers, where each layer is defined as a (110) plane that contains both Ti and O atoms. In the present calculations, a slab contains four layers (16 [$TiO_2$] units) with all the bridged oxygen atoms and the Ti atoms on top of the surface as active sites. The lower parts of the supercell are fixed at the optimized lattice constants to retain properties of the bulk $TiO_2$, and a 10 Å vacuum region is used to separate the top and bottom surfaces of the slabs to minimize the interaction between distinct slab surfaces in this infinitely periodic model system. This vacuum separation is greater than in pervious studies[46−49] and guarantees no significant interactions between the neighboring slabs. The

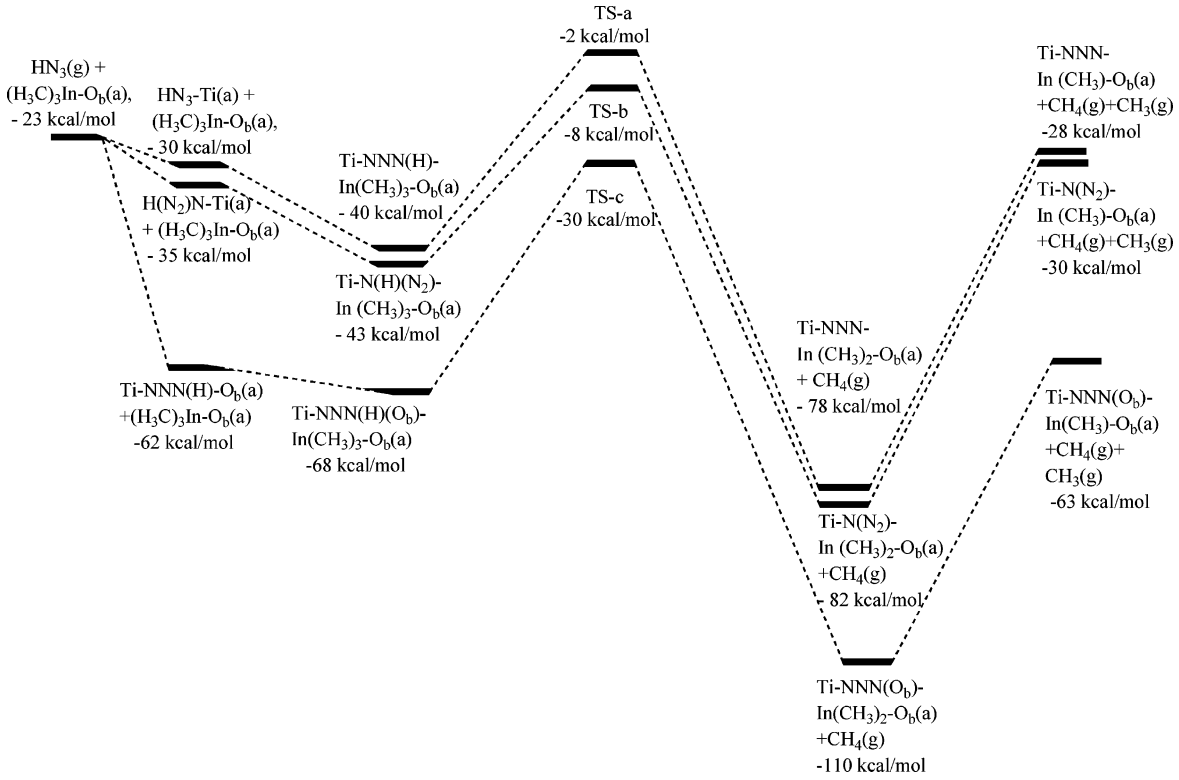


**Figure 2.** PES of the surface reactions starting with $HN_3$(a) and $(H_3C)_3In-O_b$(a) coadsorbed on the surface.

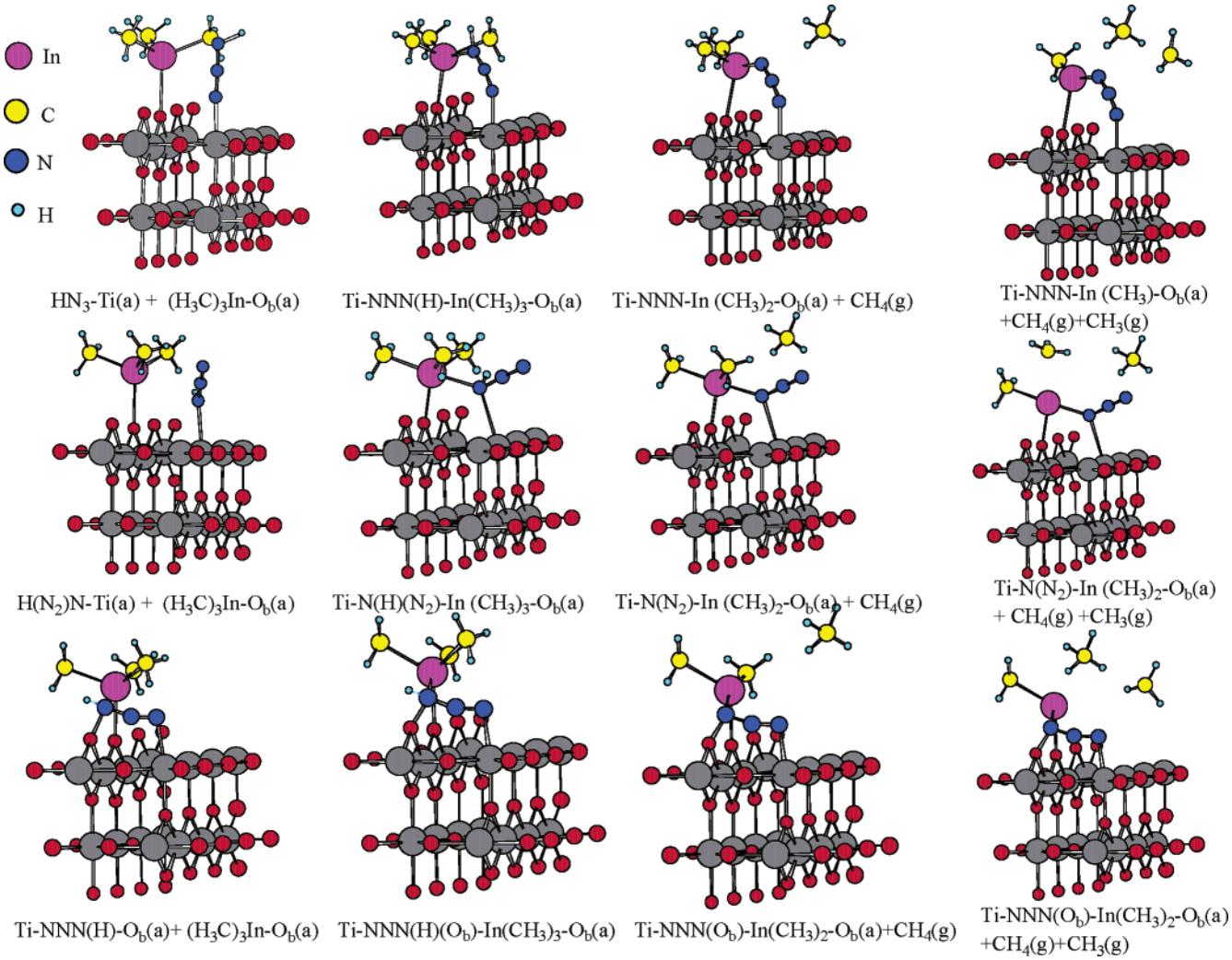


**Figure 3.** Optimized structures of possible adsorbates presented in Figure 2 displayed with two layers of $TiO_2$(110) surface model for brevity.

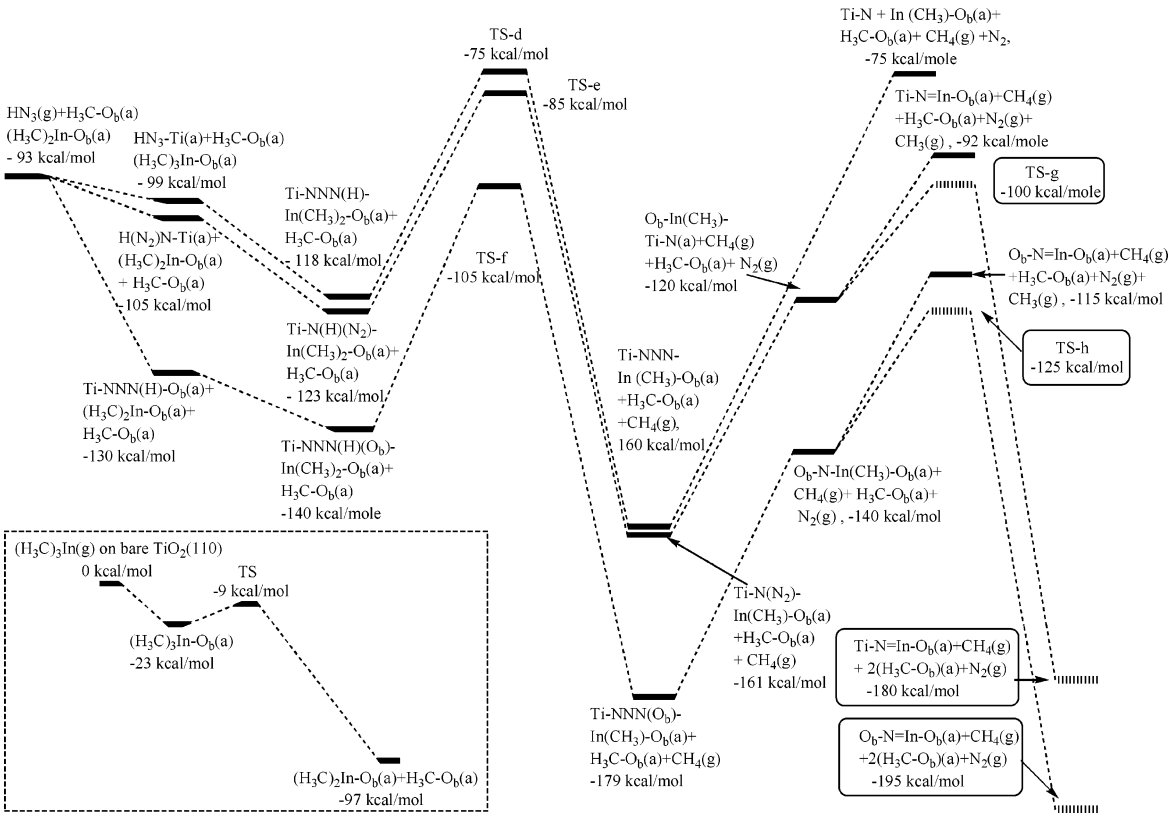


**Figure 4.** PES of the surface reactions starting with $HN_3$(a) and $(H_3C)_2In-O_b(a) + H_3C-O_b(a)$ coadsorbed on the surface. The left-bottom inset presents the dissociative adsorption of TMIn + $TiO_2$(110) forming $(H_3C)_2In-O_b(a) + H_3C-O_b(a)$ exothermically.[11]

surface area of the unit cell is 6.535 × 5.545 Å$^2$, which is also large enough to avoid the interaction between neighboring adspecies. The two neighboring adspecies have more than 2 Å distance between their edge hydrogens. The cutoff energy is kept at 600 eV, but the Monkhorst−Pack *k*-points are different, as aforementioned, 4 × 5 × 1 for the rutile (110) surfaces, because the 10 Å vacuum space is introduced in the (110) direction. This surface model had also been tested for its reliability by computing the adsorption energy of $H_2O$ on the surface as described previously.[12] The difference between the fully relaxed result, −12 kcal/mol, and the bottom layer fixed result, −20 kcal/mol (which is in close agreement with previous results[50,51]), is consistent with the trend of the infinite-slab estimation.[52−55]

**3.2. Surface Reaction Calculations.** The individual surface reactions of $HN_3$ and TMIn, the most efficient precursors for InN deposition by OMCVD, on $TiO_2$ nanoparticles have been discussed in detail experimentally and computationally,[11,12] as mentioned in the Introduction. On the basis of those results, we employ the $TiO_2$ rutile (110) surface as a model and computationally examine both the Langmuir−Hinshelwood and Rideal−Eley mechanisms for the interaction of $HN_3$ and TMIn forming InN on the surface.

As concluded in the previous studies,[11,12] on the clean rutile (110) surface, TMIn can only molecularly adsorb on a bridged O site, forming $(H_3C)_3In-O_b(a)$ with −23 kcal/mol adsorption energy.[11] By passing over a 14 kcal/mol reaction barrier, the TMIn adsorbate can dissociate to a stable product pair, $(H_3C)_2In-O_b(a) + H_3C-O_b(a)$, with −97 kcal/mol adsorption energy lying 74 kcal/mol below TMInO(a)[11] (vide infra). On the other hand, $HN_3$ can molecularly adsorb on the surface, giving three stable adsorbates with side-on and end-on configurations, $HN_3$−Ti(a), $HN(N_2)$−Ti(a) and $Ti-N_2N(H)-O_b(a)$ having −5, −8, and −36 kcal/mol adsorption energies, respectively.[12] Therefore, the combination of $(H_3C)_3In-O_b(a)$ and $(H_3C)_2In-O_b(a) + H_3C-O_b(a)$ with the three possible molecularly adsorbed $HN_3$-(a) can afford six initial reactants discussed as follows.

**a. Langmuir−Hinshelwood Mechanism.** *$(CH_3)_3InO_b(a) + HN_3(a)$.* The computed potential energy surface for the reaction of $(CH_3)_3In-O_b(a)$ with the three $HN_3(a)$ adsorbates, $HN_3$−Ti(a), $HN(N_2)$−Ti(a) and $Ti-N_2N(H)-O_b(a)$, is shown in Figure 2, and the optimized structures, presented with the partial surface model for brevity, are shown in Figure 3. The energies are all referenced to the initial reactants, $HN_3(g) + In(CH_3)_3(g) + TiO_2$ rutile (110) surface. In the initial steps, the most reactive N atom bonding with H in $HN_3$(a) can directly associate with the indium atom in $(CH_3)_3In-O_b(a)$ via barrierless and exothermic complexation processes. The exothermicities are around 6−10 kcal/mol.

From the three resulted intermediates, $Ti-NNN(H)-In(CH_3)_3-O_b(a)$, $Ti-N(H)(N_2)-In(CH_3)_3-O_b(a)$ and $Ti-NNN(H)(O_b)-In(CH_3)_3-O_b(a)$, which lie below the reactants by 40, 43 and 68 kcal/mol, the H atoms of the $HN_3$ can react with one of the methyl groups intramolecularly to eliminate $CH_4$(g), producing $Ti-NNN-In(CH_3)_2-O_b(a)$, $Ti-N(N_2)-In(CH_3)_2-O_b(a)$ and $Ti-NNN(O_b)-In(CH_3)_2-O_b(a)$ via TS-a, TS-b and TS-c, respectively. The transition states of these $CH_4$-elimination processes are very similar, located around 35−38 kcal/mol above the association complexes. These molecular-elimination processes are highly exothermic, releasing 38−42 kcal/mol of energies.

The subsequent energetically accessible reactions of the intermediates, $Ti-NNN-In(CH_3)_2-O_b(a)$, $Ti-N(N_2)-In(CH_3)_2-O_b(a)$ and $Ti-NNN(O_b)-In(CH_3)_2-O_b(a)$, are $CH_3$-elimination processes with no intrinsic barriers, producing $Ti-NNN-In(CH_3)-O_b(a)$, $Ti-N(N_2)-In(CH_3)-O_b(a)$ and $Ti-NNN(O_b)-In(CH_3)-O_b(a)$, with their overall exothermicities computed to be 28, 30 and 63 kcal/mol, respectively. These products can

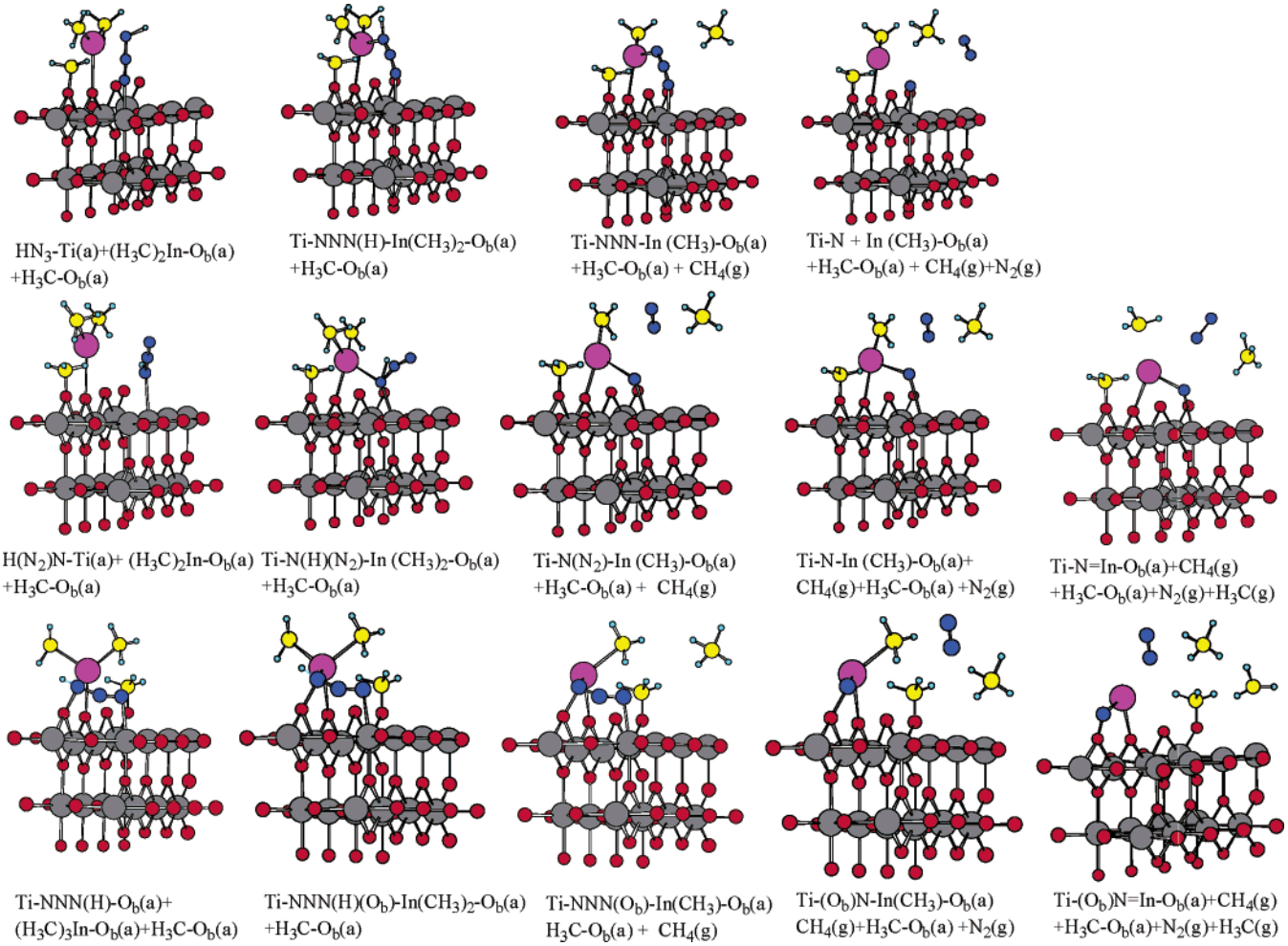


**Figure 5.** Optimized structures of possible adsorbates presented in Figure 4 displayed with two layers of $TiO_2$(110) surface model for brevity.

further decompose to give InN(a), as will be discussed in the following section on $(CH_3)_2InO_b(a) + HN_3(a)$. Alternatively, the $CH_3$ group may also migrate to a neighboring empty $O_b$ site to form $H_3C-O_b(a)$, releasing even more energy, although the additional $O_b$ sites are not shown in the model but may be available in reality.

It is worth noting that the $CH_4$-elimination processes can only occur after the In−N bonds are formed in the first step because the reaction barriers of TS-a, TS-b and TS-c are higher than the adsorption energies of either TMIn(a) or $HN_3$(a). If the In−N bonds are not formed initially, these molecular adsorbates will undergo desorption instead of the reaction to give off $CH_4$(g). In other words, the inter-adspecies reaction involving a transition state with the $Ti-N_3(H\cdots CH_3)In(CH_3)_2O_b(a)$ structure without the initial In−N bonding would have to overcome a much higher barrier.

*$(CH_3)_2InO_b(a) + HN_3(a)$.* Alternatively, the $(CH_3)_2In-O_b(a)$ formed in the highly exothermic dissociative adsorption of TMIn on $O_b$ sites, giving $(CH_3)_2In-O_b(a) + H_3C-O_b(a)$, as shown in the inset of Figure 4, can react with the three $HN_3$(a) adsorbates. The computed potential energy surface is depicted in the figure, and the optimized structures depicted with the partial surface model are presented in Figure 5. The two PES's shown in Figures 2 and 4 are very similar in the initial complexation reactions to form In−N bonds, resulting in $Ti-NNN(H)-In(CH_3)_2-O_b(a) + H_3C-O_b(a)$, $Ti-N(H)(N_2)-In(CH_3)_2-O_b(a) + H_3C-O_b(a)$ and $Ti-NNN(H)(O_b)-In(CH_3)_2-O_b(a) + H_3C-O_b(a)$, with $H_3C-O_b(a)$ formed in the initial dissociative adsorption reaction of TMIn remaining as a spectator. The exothermicities of the above three reactions, 10−19 kcal/mol, are slightly higher than those of the analogous processes involving $(H_3C)_3In-O_b(a)$, as discussed above (see Figure 2), because of the stronger In−N bonding involving $(H_3C)_2In-O_b(a)$ rather than $(H_3C)_3In-O_b(a)$ in the complexation reactions.

Following the similar $CH_4$-elimination processes, the H atoms of the $HN_3$ in the complexes can react intramolecularly with one of the $CH_3$ groups to form $CH_4$(g), yielding $Ti-NNN-In(CH_3)-O_b(a)$, $Ti-N(N_2)-In(CH_3)-O_b(a)$ and $Ti-NNN(O_b)-In(CH_3)-O_b(a)$ products together with the methoxy adsorbate, $H_3C-O_b(a)$. The barriers of these transition states presented in Figure 4, TS-d, TS-e and TS-f, lying in the range 35−43 kcal/mol, are quite close to those of TS-a, TS-b and TS-c given in Figure 2. Interestingly, these barriers are also very similar to those of $CH_4$-elimination processes, 34−37 kcal/mol, in the TMIn adsorbed on a hydroxylated rutile (110) surface.[11]

These three products are the final intermediates after $CH_3$-elimination reactions in the $(H_3C)_3In-O_b(a) + HN_3(a)$ case. Two of the resulting adsorbates, $Ti-N(N_2)-In(CH_3)-O_b(a)$ and $Ti-NNN(O_b)-In(CH_3)-O_b(a)$, can undergo direct $N_2$(g) elimination, giving rise to $Ti-N{=}In(CH_3)-O_b(a)$ and $O_b-N{=}In(CH_3)-O_b(a)$, respectively, by breaking the InN−N bonds with 39 and 41 kcal/mol endothermicities. Similar InN−N bond breaking process cannot occur in the other $Ti-NNN-In(CH_3)-O_b(a)$ adsorbate because of the high endothermicity producing $N{\equiv}In(CH_3)-O_b(a)$. Alternatively, the $N_2$-elimination process can still occur by breaking the TiN−N bond, producing $N-Ti(a) + In(CH_3)-O_b(a)$ with an endothermicity of 85 kcal/mol

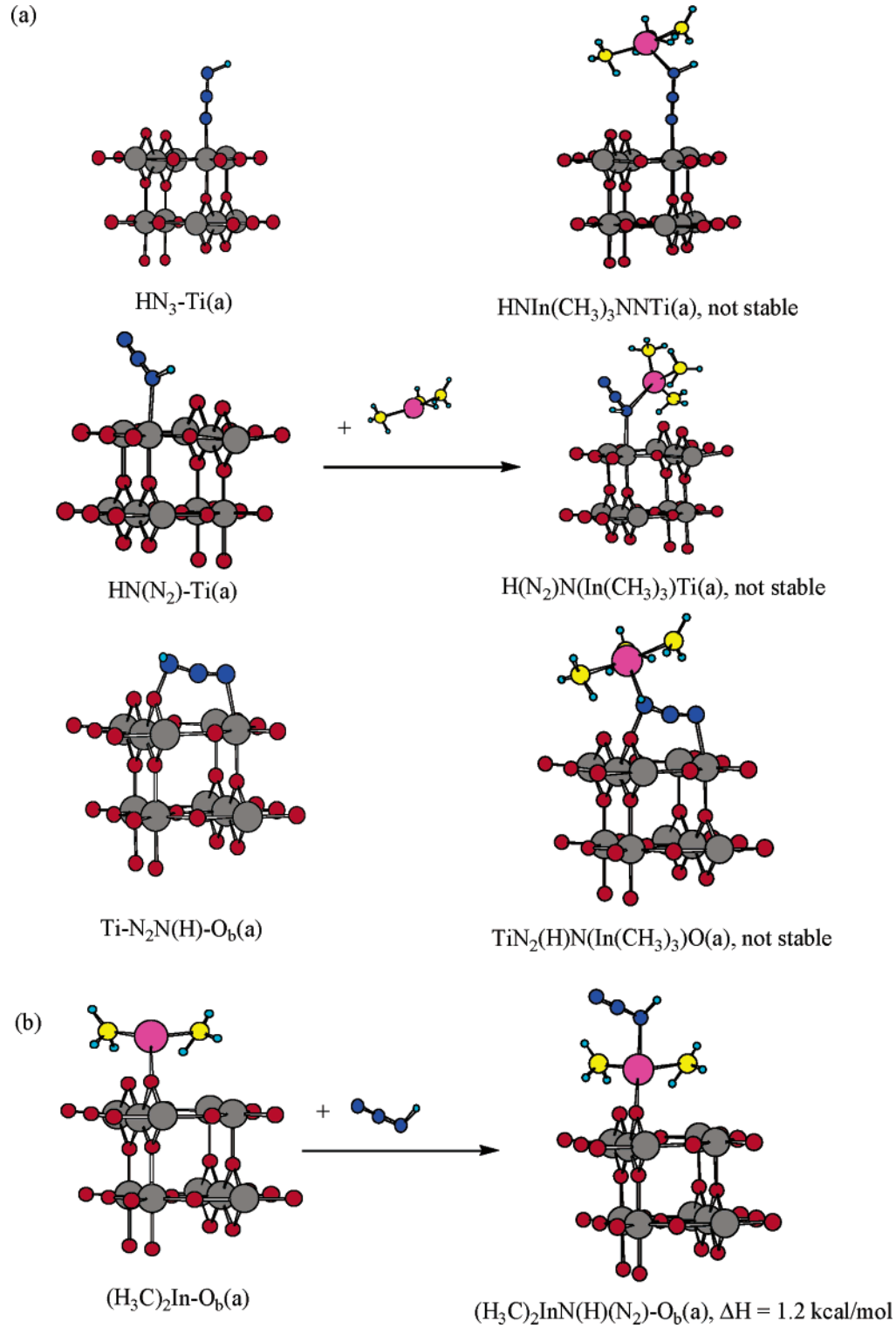


**Figure 6.** Two cases of the Rideal−Eley mechanism: (a) $HN_3$(a) + TMIn(g); (b) TMIn(a) + $HN_3$(a).

and the overall exothermicity of 75 kcal/mol (see Figure 4). It should be mentioned that there might exist intrinsic transition states in these $N_2$-elimination processes. However, an extensive search for them was not successful.

As shown in Figure 4, Ti−N═In($CH_3$)−$O_b$(a) and $O_b$−N═In($CH_3$)−$O_b$(a), which are considered as the likely precursors of InN(a) formation, can undergo methyl-elimination or methyl-migration reactions (to available unoccupied $O_b$ sites nearby) to produce InN(a) with double (side-on) adsorption configurations, Ti−N═In−$O_b$(a) and $O_b$−N═In−$O_b$(a), respectively, which are computed to be the most stable InN adspecies, as presented in section 3.3. The two methyl-elimination reactions, Ti−N═In($CH_3$)−$O_b$(a) → Ti−N═In−$O_b$(a) + $CH_3$(g) and $O_b$−N═In($CH_3$)−$O_b$(a) → $O_b$−N═In−$O_b$(a) + $CH_3$(g), have no intrinsic reaction barriers, similar to the decomposition reactions, Ti−NNN−In($CH_3$)$_2$−$O_b$(a) → Ti−NNN−In($CH_3$)−$O_b$(a) + $CH_3$(g), etc., shown in Figure 2, with endothermicities in the range 25−28 kcal/mol.

The migration of the $CH_3$ group in Ti−N═In($CH_3$)−$O_b$(a) → TS-g → Ti−N═In−$O_b$(a) + $H_3C$−$O_b$(a) and $O_b$−N═In-($CH_3$)−$O_b$(a) → TS-h → $O_b$−N═In−$O_b$(a) + $H_3C$−$O_b$(a) takes place with reaction barriers of 20 and 15 kcal/mol, and the high

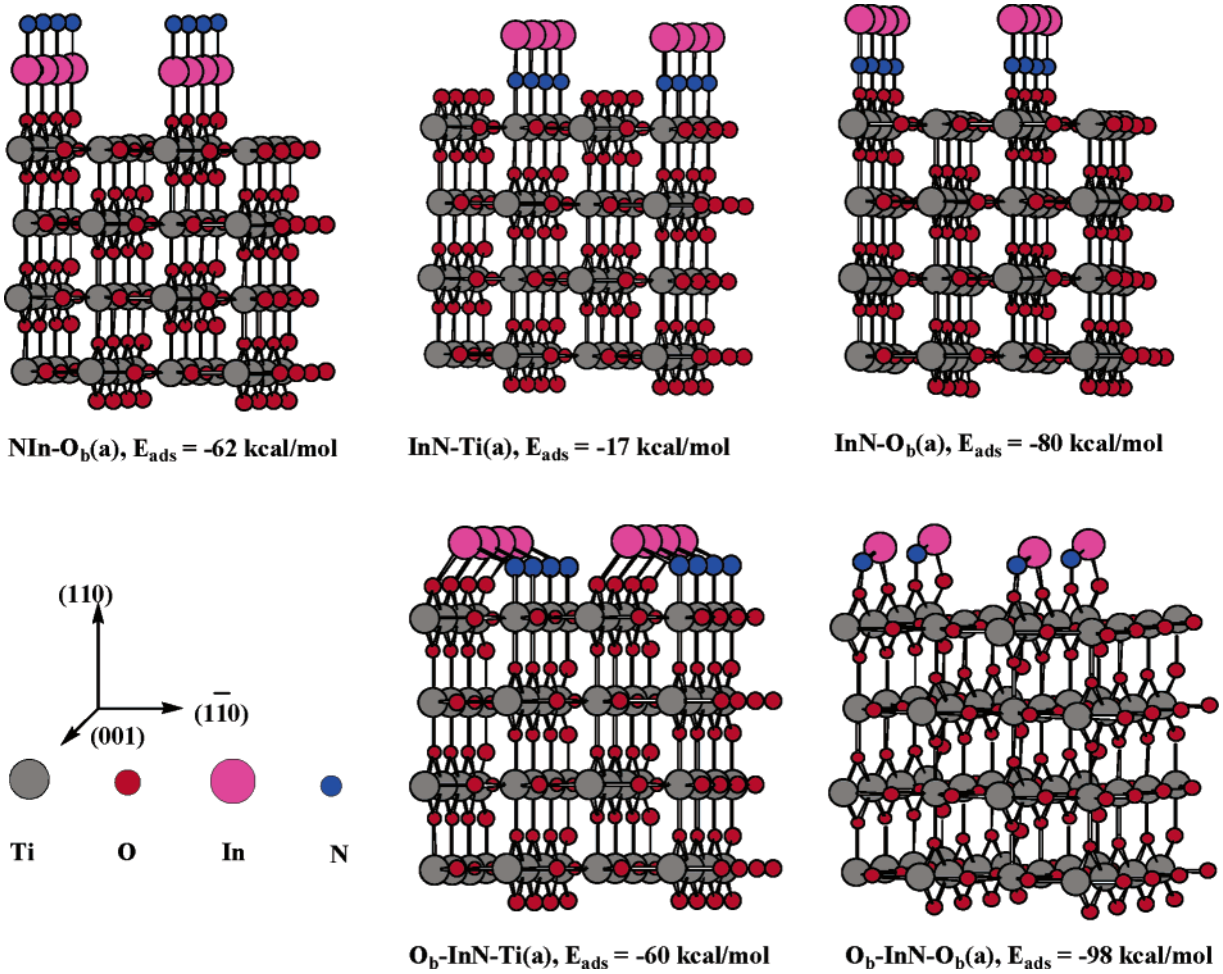


**Figure 7.** Geometrical structures and adsorption energies, $E_{ads} = (E_{total} - nE_{molecule} - E_{surface})/n$, where $n$ equals the number of adsorbed InN molecules.

exothermicities of 60 and 55 kcal/mol, respectively, producing side-on InN adsorbates with different configurations, as shown in Figure 4. These results are consistent with the methyl-migration processes in the TMIn/rutile (110) system.[11]

*b. Rideal−Eley Mechanism.* Two possible processes that may take place by the Rideal−Eley mechanism are considered for comparison: $HN_3$(a) + TMIn(g) and $HN_3$(g) + TMIn(a), as shown in Figure 6. In the first case, the three $HN_3$(a) adsorbates, $HN_3$−Ti(a), HN($N_2$)−Ti(a) and Ti−$N_2$N(H)−$O_b$(a), were studied as the initial reactants. To form the InN(a) product, the In atom has to bond with the most reactive N atom bonding with H in $HN_3$(a), forming $(CH_3)_3$InN(H)NNTi(a), $(CH_3)_3$InN(H)-($N_2$)Ti(a) and Ti$N_2$N(H)(In$(CH_3)_3$)O(a). However, these intermediates are not stable because the nitrogen atoms are over-coordinated.

In the second case, the only possible reaction is $(H_3C)_2InO_b$-(a) reacting with $HN_3$(g) to form $(CH_3)_2$InN(H)($N_2$)$O_b$(a). This process forms a weak In−N bond with 1.2 kcal/mol binding energy. In the following step, the H atom (bonded to N) can react with one of the $CH_3$ groups to produce $CH_4$(g). The barrier of this transition state was predicted to be rather high, 33 kcal/mol, above the weak complex. The $CH_4$-elimination process is, therefore, not competitive with the desorption of the $HN_3$ from the weak complex.

Accordingly, the above two cases show that InN(a) cannot be formed favorably by the Rideal−Eley type reactions. On the other hand, the two possible structures of InN(a), Ti−N═In−$O_b$(a) and $O_b$−N═In−$O_b$(a), can be produced by the Langmuir−Hinshelwood mechanism with very high exothermicities, as discussed in the preceding section.

**3.3. InN Adsorption Structures.** To confirm the InN adsorbates formed by the reactions discussed above, possible adsorption structures and energies of InN(a) on $TiO_2$ rutile (110) surface have been computed without other species. Three end-on and two side-on adsorption structures have been found, as shown in Figure 7. Among these adsorption structures, the In atom can form a strong bond, 62 kcal/mol, with the 2-fold-coordinated bridged O atom, but not with the 5-fold-coordinated surface Ti atom. This is consistent with the results of the TMIn/rutile (110) system we recently studied.[11] On the other hand, as in the HN−rutile bonding discussed in the $HN_3$/rutile (110) system,[12] the N atom of InN can form a stronger bond with the 2-fold-coordinated O atom with an 80 kcal/mol binding energy than with the 5-fold-coordinated Ti atom with a 17 kcal/mol binding energy in the end-on adsorption configuration. In addition, InN also has two double (side-on) adsorption configurations on the surface: the $O_b$−InN−Ti(a) structure with a slightly weaker Ti−N bond has a smaller adsorption energy, −60 kcal/mol, than that of the $O_b$−InN−$O_b$(a) structure with a stronger $O_b$−N bond, −98 kcal/mol. As computed in section 3.2, the three less stable end-on adsorptions cannot be readily formed on the surface because of the energetically unfavored Rideal−Eley mechanism. On the other hand, the two more stable side-on adsorptions are easily formed following the Langmuir−Hinshelwood mechanism.

## 4. Summary

In this work, the reactions of $HN_3$ and TMIn coadsorbed on the $TiO_2$ rutile (110) surface have been computationally studied by first-principles calculations. The potential energy surfaces and the mechanisms of the reactions involving the three stable $HN_3$ adsorbates, $HN_3-Ti(a)$, $HN(N_2)-Ti(a)$, and $Ti-N_2N(H)-O_b(a)$, with $(H_3C)_xIn-O_b(a)$ ($x = 2, 3$) have been explicitly examined.

When $HN_3(a)$ and $(H_3C)_xIn-O_b(a)$ adsorbed at neighboring active sites, their reactions may begin with the exothermic N−In complexation processes. The resulting $HN_3-In(CH_3)_x(a)$ complexes are predicted to have large adsorption energies and are possible to overcome the barriers for direct $CH_4$-elimination processes producing stable $Ti-N_3-In(CH_3)_{x-1}(a)$ intermediates with estimated exothermicities of ∼40 kcal/mol. Furthermore, two of these intermediates, $Ti-N(N_2)-In(CH_3)-O_b(a)$ and $Ti-NNN(O_b)-In(CH_3)-O_b(a)$, can dissociate at the InN−N bond to form $Ti-N-In(CH_3)-O_b(a)$ and $O_b-N-In(CH_3)-O_b(a)$, respectively. The elimination or migration of the $CH_3$ group with relatively small reaction endothermicities or barriers (<28 kcal/mol), finally gives rise to the stable side-on InN(a) adsorbates, $Ti-N=In-O_b(a)$ and $O_b-N=In-O_b(a)$, on the $TiO_2$ surface with very large overall exothermicities (>180 kcal/mol). A similar study of the reactions of $HN_3$ with TMIn by the Rideal−Eley mechanism, $HN_3(a)$ + TMIn(g) and $HN_3(g)$ + TMIn(a), shows that they are energetically less favorable than the aforementioned Langmuir−Hinshelwood processes, producing two most stable InN(a) side-on adsorption configurations.

**Acknowledgment.** J.H.W. is grateful for the support from the Graduate School of Emory University and M.C.L. acknowledges the support from the R. W. Woodruff Professorship at Emory University and from Taiwan's National Science Council for a Distinguished Visiting Professorship at the Center for Interdisciplinary Molecular Science, National Chiao Tung University, Hsinchu, Taiwan. We are also grateful to Taiwan's National Center for High-performance Computing for the use of its computational facility through the Taiwan Computational Chemistry Consortium funded by the Institute of Nuclear Energy Research Project No. NL940251.

## References and Notes

(1) Irie, H.; Watanabe, Y.; Hashimoto, K. *J. Phys. Chem. B* **2003**, *107*, 5483.
(2) Asahi, R.; Morikawa, T.; Ohwaki, T.; Aoki, K.; Taga, Y. *Science* **2001**, *293*, 269.
(3) Burda, C.; Lou, Y.; Chen, X.; Samia, A. C. S.; Stout, J.; Gole, J. L. *Nano Lett.* **2003**, *3*, 1049.
(4) Graetzel, M. *Nature* **2001**, *414*, 338.
(5) Nedeljkovic, J. M.; Micic, O. L.; Ahrenkiel, P.; Miedaner, A.; Nozik, A. J. *J. Am. Chem. Soc.* **2004**, *126*, 2632.
(6) Wang, J. H.; Lin, M. C. *ChemPhysChem* **2004**, *5*, 1615.
(7) Bu, Y.; Ma, L.; Lin, M. C. *J. Vac. Sci. Technol. A* **1993**, *11*, 2931.
(8) Bu, Y.; Lin, M. C. *Mater. Res. Soc. Symp. Proc.* **1993**, *335*, 21.
(9) Wakahara, A.; Tsuchiya, T.; Yoshida, A. *J. Cryst. Growth* **1990**, *99*, 385.
(10) Nazeeruddin, M.-K.; Kay, A.; Rodicio, I.; Humphry-Baker, R.; Muller, E.; Liska, P.; Vlachopoulos, N.; Graetzel, M. *J. Am. Chem. Soc.* **1993**, *115*, 6328.
(11) Wang, J. H.; Lin, M. C. *J. Phys. Chem. B* **2005**, *109*, 20858.
(12) Wang, J. H.; Lin, M. C.; Sun, Y. C. *J. Phys. Chem. B* **2005**, *109*, 5133.
(13) Carlo, S. R.; Torres, J.; Fairbrother, D. H. *J. Phys. Chem. B* **2001**, *105*, 6148.
(14) Thoms, B. D.; Russell, J. N., Jr. *Surf. Sci.* **1995**, *337*, L807.
(15) Bu, Y.; Lin, M. C. *Surf. Sci.* **1994**, *317*, 152.
(16) Chu, J. C. S.; Bu, Y.; Lin, M. C. *Mater. Lett.* **1992**, *14*, 207.
(17) Chu, J. C. S.; Bu, Y.; Lin, M. C. *Surf. Sci.* **1993**, *284*, 281.
(18) Bu, Y.; Lin, M. C. *Surf. Sci.* **1994**, *301*, 118.
(19) Russell, J. N., Jr.; Bermudez, V. M.; Leming, A. *Langmuir* **1996**, *12*, 6492.
(20) Shogen, S.; Matsumi, Y.; Kawasaki, M. *Thin Solid Films* **1992**, *218*, 58.
(21) Bu, Y.; Chu, J. C. S.; Lin, M. C. *Mater. Lett.* **1992**, *14*, 207.
(22) Horwitz, J. S.; Villa, E.; Hsu, D. S. Y. *J. Phys. Chem.* **1990**, *94*, 7214.
(23) Villa, E.; Horwitz, J. S.; Hsu, D. S. Y. *Chem. Phys. Lett.* **1989**, *164*, 587.
(24) Aquino, A. A.; Mulcahy, C. P. A.; Jones, T. S. *Surf. Sci.* **1995**, *344*, L1231.
(25) Aquino, A. A.; Mulcahy, C. P. A.; Jones, T. S. *Chem. Phys. Lett.* **1996**, *252*, 159.
(26) Donnelly, V. M.; McCaulley, J. A. *Surf. Sci.* **1990**, *235*, L333.
(27) Shogen, S.; Ohashi, M.; Hashimoto, S.; Kawasaki, M.; Hosokawa, Y. *Mater. Res. Soc. Symp. Proc.* **1993**, *280*, 193.
(28) Rusu, C. N.; Yates, J., J. T. *J. Phys. Chem. B* **2000**, *104*, 12299.
(29) Chuang, C.-C.; Chen, C.-C.; Lin, J.-L. *J. Phys. Chem. B* **1999**, *103*, 2439.
(30) Wu, W.-C.; Chuang, C.-C.; Lin, J.-L. *J. Phys. Chem. B* **2000**, *104*, 8719.
(31) Liao, L.-F.; Wu, W.-C.; Chuang, C.-C.; Lin, J.-L. *J. Phys. Chem. B* **2001**, *105*, 5928.
(32) Kresse, G.; Hafner, J. *Phys. Rev. B* **1993**, *47*, 558.
(33) Kresse, G.; Hafner, J. *Phys. Rev. B* **1994**, *49*, 14251.
(34) Kresse, G.; Furthmuller, J. *Comput. Mater. Sci.* **1996**, *6*, 15.
(35) Kresse, G.; Furthmuller, J. *Phys. Rev. B* **1996**, *54*, 11169.
(36) Cleperley, D. M.; Alder, B. J. *Phys. Rev. Lett.* **1980**, *45*, 566.
(37) Perdew, J. P.; Yang, Y. *Phys. Rev. B* **1992**, *45*, 244.
(38) Perdew, J. P.; Chevary, J. A.; Vosko, S. H.; Jackson, K. A.; Penderson, M. R.; Singh, D. J.; Fiolhais, C. *Phys. Rev. B* **1992**, *46*, 6671.
(39) Lee, C.; Yang, W.; Parr, R. G. *Phys. Rev. B* **1988**, *37*, 785.
(40) Herman, G. S.; Dohnalek, Z.; Ruzycki, N.; Diebold, U. *J. Phys. Chem. B* **2003**, *107*, 2788.
(41) Li, W.; Ni, C.; Lin, H. C.; P., H. C.; Shah, S. I. *J. Appl. Phys.* **2004**, *96*, 6663.
(42) McCormick, J. R.; Zhao, B.; Rykov, S. A.; Wang, H.; Chen, G. *J. Phys. Chem. B* **2004**, *108*, 17398.
(43) Wyckoff, R. W. G. *Crystal Structure*, 2nd ed.; Wiley: New York, 1964; Vol. 1.
(44) Monkhorst, H.; Pack, J. *Phys. Rev. B* **1976**, *13*, 5188.
(45) Mills, G.; Jonsson, H.; Schenter, G. K. *Surf. Sci.* **1995**, *324*, 305.
(46) Rasmussen, M. D.; Molina, L. M.; Hammer, B. *J. Chem. Phys.* **2004**, *120*, 988.
(47) Rego, L. G. C.; Batista, V. S. *J. Am. Chem. Soc.* **2003**, *125*, 7989.
(48) Menetrey, M.; Markovits, A.; Minot, C. *Surf. Sci.* **2003**, *524*, 49.
(49) Sorescu, D. C.; Rusu, C. N.; Yates, J., John T. *J. Phys. Chem. B* **2000**, *104*, 4408.
(50) Lindan, P. J. D.; Harrison, N. M. *Phys. Rev. Lett.* **1998**, *80*, 762.
(51) Goniakowski, J.; Gillan, M. J. *Surf. Sci.* **1996**, *350*, 145.
(52) Harris, L. A.; Quong, A. A. *Phys. Rev. Lett.* **2004**, *93*, 086105.
(53) Egerton, T. A.; Tooley, I. R. *J. Phys. Chem. B* **2004**, *108*, 5066.
(54) Fujisjima, A.; Hashaimoto, K.; Watanabe, T. *TiO2 Photocatalysis: Fundamentals and Applications*; Bkc, Inc.: Tokyo, 1999.
(55) Ollis, D.; El-Akabi, H. *Photocatalytic Purification and Treatment of Water and Air*; Elsevier: New York, 1993.